Resummation

G. Altarelli, J. Andersen, R. D. Ball, M. Ciafaloni, D. Colferai, G. Corcella, S. Forte, L. Magnea, A. Sabio Vera, G. P. Salam, A. Staśto

1 Introduction [1]

An accurate perturbative determination of the hard partonic cross-sections (coefficient functions) and of the anomalous dimensions which govern parton evolution is necessary for the precise extraction of parton densities. Recent progress in the determination of higher order contributions to these quantities has been reviewed in [1]. As is well known, such high-order perturbative calculations display classes of terms containing large logarithms, which ultimately signal the breakdown of perturbation theory. Because these terms are scale–dependent and in general non universal, lack of their inclusion can lead to significant distortion of the parton densities in some kinematical regions, thereby leading to loss of accuracy if parton distributions extracted from deep-inelastic scattering (DIS) or the Drell-Yan (DY) processes are used at the LHC.

Logarithimic enhancement of higher order perturbative contribution may take place when more than one large scale ratio is present. In DIS and DY this happen in the two opposite limits when the center-of-mass energy of the partonic collision is much higher than the characteristic scale of the process, or close to the threshold for the production of the final state. These correspond respectively to the small x and large x kinematical regions, where $0 \leq x \leq 1$ is defined in terms of the invariant mass M^2 of the non-leptonic final state as $M^2 = \frac{(1-x)Q^2}{x}$. The corresponding perturbative contributions are respectively enhanced by powers of $\ln \frac{1}{x}$ and $\ln(1-x)$, or, equivalently, in the space of Mellin moments, by powers of $\frac{1}{N}$ and $\ln N$, where $N \to 0$ moments dominate as $x \to 0$ while $N \to \infty$ moments dominate as $x \to 1$.

The theoretical status of small x and large x resummation is somewhat different. Large x logs are well understood and the corresponding perturbative corrections have been determined to all orders with very high accuracy. Indeed, the coefficients that determine their resummation can be extracted from fixed-order perturbative computations. Their resummation for DY and DIS was originally derived in [2, 3] and extended on very general grounds in [4]. The coefficients of the resulting exponentiation have now been determined so that resummation can now be performed exactly at $\mathrm{N^2LL}$ [5, 6], and to a very good approximation at $\mathrm{N^3LL}$ [7–9], including even some non-logarithmic terms [10]. On the other hand, small x logs are due to the fact that at high energies, due to the opening of phase space, both collinear [11–13] and high-energy [14–17] logarithms contribute, and thus the coefficients required for their resummation can only be extracted from a simultaneous resolution of the DGLAP equation, which resums collinear logarithms, and the BFKL equation, which resum the high-energy logarithms. Although the determination of the kernels of these two equations has dramatically progressed in the last several years, thanks to the computation of the $\mathrm{N^2LO}$ DGLAP kernel [6, 18] and of the NLO BFKL kernel [14–17, 19, 20], the formalism which is needed to combine these two equations, as required for sucessful phenomenology, has only recently progressed to the point of being usable for realistic applications [21–30].

In practice, however, neither small x nor large x resummation is systematically incorporated in current parton fits, so data points for which such effects may be important must be discarded. This is especially unsatisfactory in the case of large x resummation, where resummed results (albeit with a varying degree of logarithmic accuracy) are available for essentially all processes of interest for a global parton fit, in particular, besides DIS and DY, prompt photon production [31, 32], jet production [33, 34] and heavy quark electroproduction [35,36]. Even if one were to conclude that resummation is not needed, either because (at small x) it is affected by theoretical uncertainties or because (at large x) its effects are

[1] Subsection coordinator: S. Forte

small, this conclusion could only be arrived at after a careful study of the impact of resummation on the determination of parton distributions, which is not available so far.

The purpose of this section is to provide a first assessment of the potential impact of the inclusion of small x and large x resummation on the determination of parton distributions. In the case of large x, this will be done by determining resummation effects on parton distributions extracted from structure functions within a simplified parton fit. In the case of small x, this will be done through a study of the impact of small x resummation on splitting functions, as well as the theoretical uncertainty involved in the resummation process, in particular by comparing the results obtained within the approach of ref. [21–23] and that of ref. [24–30]. We will also discuss numerical approaches to the solution of the small-x (BFKL) evolution equation.

2 Soft gluons

With the current level of theoretical control of soft gluon resummations, available calculations for DIS or DY should be fully reliable over most of the available phase space. Specifically, one expects current (resummed) predictions for DIS structure functions to apply so long as the leading power correction can be neglected, *i.e.* so long as $W^2 \sim (1-x)Q^2 >> \Lambda^2$, with $x = x_{Bj}$. Similarly, for the inclusive DY cross section, one would expect the same to be true so long as $(1-z)^2Q^2 >> \Lambda^2$, where now $z = Q^2/\hat{s}$, with $\hat{s} = x_1 x_2 S$ the partonic center of mass energy squared. Indeed, as already mentioned, a consistent inclusion of resummation effects in parton fits is feasible with present knowledge: on the one hand, recent fits show that consistent parton sets can be obtained by making use of data from a single process (DIS) (see [37,38] and Ref. [39]), on the other hand, even if one adopts the philosophy of global fits, resummed calculations are available for all processes of interest.

In practice, however, currently available global parton fits are based on NLO, or $\mathrm{N^2LO}$ fixed-order perturbative calculations, so data points which would lie within the expected reach of resummed calculations cannot be fit consistently and must be discarded. The effect is that large-x quark distributions become less constrained, which has consequences on the gluon distribution, as well as on medium-x quark distributions, through sum rules and evolution. The pool of untapped information is growing, as more data at large values of x have become available from, say, the NuTeV collaboration at Fermilab [40, 41]. A related issue is the fact that a growing number of QCD predictions for various processes of interest at the LHC are now computed including resummation effects in the hard partonic cross sections, which must be convoluted with parton densities in order to make predictions at hadron level. Such predictions are not fully consistent, since higher order effects are taken into account at parton level, but disregarded in defining the parton content of the colliding hadrons.

It is therefore worthwile to provide an assessment of the potential impact of resummation on parton distributions. Here, we will do this by computing resummation effects on quark distributions in the context of a simplified parton fit.

2.1 General Formalism in DIS

Deep Inelastic Scattering structure functions $F_i(x,Q^2)$ are given by the convolution of perturbative coefficient functions, typically given in the $\overline{\mathrm{MS}}$ factorization scheme, and parton densities. The coefficient functions C_i^q for quark-initiated DIS present terms that become large when the Bjorken variable x for the partonic process is close to $x = 1$, which forces gluon radiation from the incoming quark to be soft or collinear. At $\mathcal{O}(\alpha_s)$, for example, the coefficient functions can be written in the form

$$C_i^q\left(x, \frac{Q^2}{\mu_F^2}, \alpha_s(\mu^2)\right) = \delta(1-x) + \frac{\alpha_s(\mu^2)}{2\pi} H_i^q\left(x, \frac{Q^2}{\mu_F^2}\right) + \mathcal{O}\left(\alpha_s^2\right) . \tag{1}$$

Treating all quarks as massless, the part of H_i^q which contains terms that are logarithmically enhanced as $x \to 1$ reads

$$H^q_{i,\rm soft}\left(x,\frac{Q^2}{\mu_F^2}\right) = 2C_F\left\{\left[\frac{\ln(1-x)}{1-x}\right]_+ + \frac{1}{(1-x)_+}\left(\frac{\ln Q^2}{\mu_F^2}-\frac{3}{4}\right)\right\}. \tag{2}$$

In moment space, where soft resummation is naturally performed, the contributions proportional to $\alpha_s[\ln(1-x)/(1-x)]_+$ and to $\alpha_s[1/(1-x)]_+$ correspond to double $(\alpha_s \ln^2 N)$ and single $(\alpha_s \ln N)$ logarithms of the Mellin variable N. The Mellin transform of Eq. (2) in fact reads, at large N,

$$\hat{H}^q_{i,\rm soft}\left(N,\frac{Q^2}{\mu_F^2}\right) = 2C_F\left\{\frac{1}{2}\ln^2 N + \left[\gamma_E + \frac{3}{4} - \frac{\ln Q^2}{\mu_F^2}\right]\ln N\right\}. \tag{3}$$

All terms growing logarithmically with N, as well as all N-independent terms corresponding to contributions proportional to $\delta(1-x)$ in x-space, have been shown to exponentiate. In particular, the pattern of exponentiation of logarithmic singularities is nontrivial: one finds that the coefficient functions can be written as

$$\hat{C}_i^q\left(N,\frac{Q^2}{\mu_F^2},\alpha_s(\mu^2)\right) = \mathcal{R}\left(N,\frac{Q^2}{\mu_F^2},\alpha_s(\mu^2)\right)\Delta\left(N,\frac{Q^2}{\mu_F^2},\alpha_s(\mu^2)\right), \tag{4}$$

where $\mathcal{R}(N, Q^2/\mu_F^2, \alpha_s(\mu^2))$ is a finite remainder, nonsingular as $N \to \infty$, while [4]

$$\ln\Delta\left(N,\frac{Q^2}{\mu_F^2},\alpha_s(\mu^2)\right) = \int_0^1 dx \frac{x^{N-1}-1}{1-x}\left\{\int_{\mu_F^2}^{(1-x)Q^2}\frac{dk^2}{k^2}A\left[\alpha_s(k^2)\right] + B\left[\alpha_s\left(Q^2(1-x)\right)\right]\right\}. \tag{5}$$

In Eq. (5) the leading logarithms (LL), of the form $\alpha_s^n \ln^{n+1} N$, are generated at each order by the function A. Next-to-leading logarithms (NLL), on the other hand, of the form $\alpha_s^n \ln^n N$, require the knowledge of the function B. In general, resumming $\mathrm{N}^k\mathrm{LL}$ to all orders requires the knowledge of the function A to $k+1$ loops, and of the function B to k loops. In the following, we will adopt the common standard of NLL resummation, therefore we need the expansions

$$A(\alpha_s) = \sum_{n=1}^{\infty}\left(\frac{\alpha_s}{\pi}\right)^n A^{(n)} \;\;;\;\; B(\alpha_s) = \sum_{n=1}^{\infty}\left(\frac{\alpha_s}{\pi}\right)^n B^{(n)} \tag{6}$$

to second order for A and to first order for B. The relevant coefficients are

$$\begin{aligned} A^{(1)} &= C_F\,, \\ A^{(2)} &= \frac{1}{2}C_F\left[C_A\left(\frac{67}{18}-\frac{\pi^2}{6}\right)-\frac{5}{9}n_f\right], \\ B^{(1)} &= -\frac{3}{4}C_F\,. \end{aligned} \tag{7}$$

Notice that in Eq. (5) the term $\sim A(\alpha_s(k^2))/k^2$ resums the contributions of gluons that are both soft and collinear, and in fact the anomalous dimension A can be extracted order by order from the residue of the singularity of the nonsinglet splitting function as $x \to 1$. The function B, on the other hand, is related to collinear emission from the final state current jet.

In [35, 36] soft resummation was extended to the case of heavy quark production in DIS. In the case of heavy quarks, the function $B(\alpha_s)$ needs to be replaced by a different function, called $S(\alpha_s)$ in [36], which is characteristic of processes with massive quarks, and includes effects of large-angle soft radiation. In the following, we shall consider values of Q^2 much larger than the quark masses and employ the resummation results in the massless approximation, as given in Eq. (5).

2.2 Simplified parton fit

We would like to use large-x resummation in the DIS coefficient functions to extract resummed parton densities from DIS structure function data. Large-x data typically come from fixed-target experiments: in the following, we shall consider recent charged-current (CC) data from neutrino-iron scattering, collected by the NuTeV collaboration [40, 41], and neutral-current (NC) data from the NMC [42] and BCDMS [43, 44] collaborations.

Our strategy will be to make use of data at different, fixed values of Q^2. We will extract from these data moments of the corresponding structure functions, with errors; since such moments factor into a product of moments of parton densities times moments of coefficient functions, computing parton moments with errors is straightforward. We then compare NLO to resummed partons in Mellin space, and subsequently provide a translation back to x-space by means of simple parametrization. Clearly, given the limited data set we are working with, our results will be affected by comparatively large errors, and we will have to make simplifying assumptions in order to isolate specific quark densities. Resummation effects are, however, clearly visible, and we believe that our fit provides a rough quantitative estimate of their size. A more precise quantitative analysis would have to be performed in the context of a global fit.

The first step is to construct a parametrization of the chosen data. An efficient and faithful parametrization of the NMC and BCDMS neutral-current structure functions was provided in [45, 46], where a large sample of Monte Carlo copies of the original data was generated, taking properly into account errors and correlations, and a neural network was trained on each copy of the data. One can then use the ensemble of networks as a faithful and unbiased representation of the probability distribution in the space of structure functions. We shall make use of the nonsinglet structure function $F_2^{\rm ns}(x,Q^2)$ extracted from these data, as it is unaffected by gluon contributions, and provides a combination of up and down quark densities which is independent of the ones we extract from charged current data (specifically, $F_2^{\rm ns}(x,Q^2)$ gives $u-d$).

As far as the NuTeV data are concerned, we shall consider the data on the CC structure functions F_2 and F_3. The structure function F_3 can be written as a convolution of the coefficient function C_3^q with quark and antiquark distributions, with no gluon contribution, as

$$xF_3 = \frac{1}{2}\left(xF_3^{\nu} + xF_3^{\bar\nu}\right) = x\left[\sum_{q,q'} |V_{qq'}|^2 \left(q-\bar q\right)\otimes C_3^q\right] . \tag{8}$$

We consider data for F_3 at $Q^2 = 12.59$ and 31.62 GeV^2, and, in order to compute moments, we fit them using the functional form

$$xF_3(x) = Cx^{-\rho}(1-x)^{\sigma}(1+kx) . \tag{9}$$

The best-fit values of C, ρ and δ, along with the χ^2 per degree of freedom, are given in [47]. Here we show the relevant NuTeV data on xF_3, along with our best-fit curves, in Fig. 1.

The analysis of NuTeV data on F_2 is slightly complicated by the fact that gluon-initiated DIS gives a contribution, which, however, is not enhanced but suppressed at large x. We proceed therefore by taking the gluon density from a global fit, such as the NLO set CTEQ6M [48], and subtract from F_2 the gluon contribution point by point. We then write F_2 as

$$F_2 \equiv \frac{1}{2}\left(F_2^{\nu} + F_2^{\bar\nu}\right) = x\sum_{q,q'} |V_{qq'}|^2 \left[(q+\bar q)\otimes C_2^q + g\otimes C_2^g\right] \equiv F_2^q + F_2^g , \tag{10}$$

and fit only the quark-initiated part F_2^q, using the same parametrization as in Eq. (9). Fig. 2 shows the data on F_2^q and the best fit curves, as determined in Ref. [47]. After the subtraction of the gluon contribution from F_2, the structure functions we are considering (F_2^q, xF_3 and $F_2^{\rm ns}$) are all given in factorized form as

$$F_i(x,Q^2) = x\int_x^1 \frac{d\xi}{\xi}\, q_i\left(\xi,\mu_F^2\right) C_i^q\left(\frac{x}{\xi}, \frac{Q^2}{\mu_F^2}, \alpha_s(\mu^2)\right) , \tag{11}$$

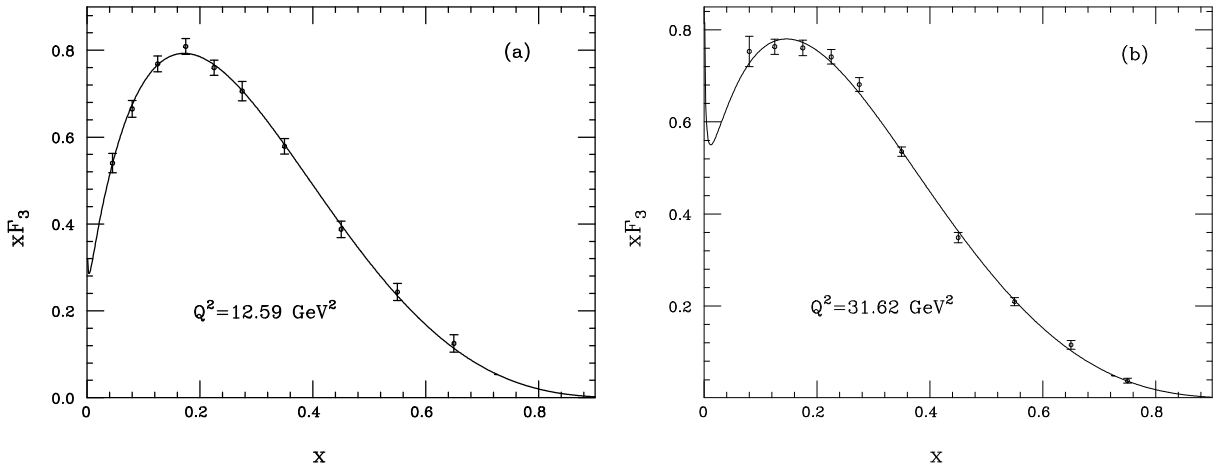

Fig. 1: NuTeV data on the structure function xF_3, at $Q^2 = 12.59\ \mathrm{GeV}^2$ (a) and at $Q^2 = 31.62\ \mathrm{GeV}^2$ (b), along with the best fit curve parametrized by Eq. (9).

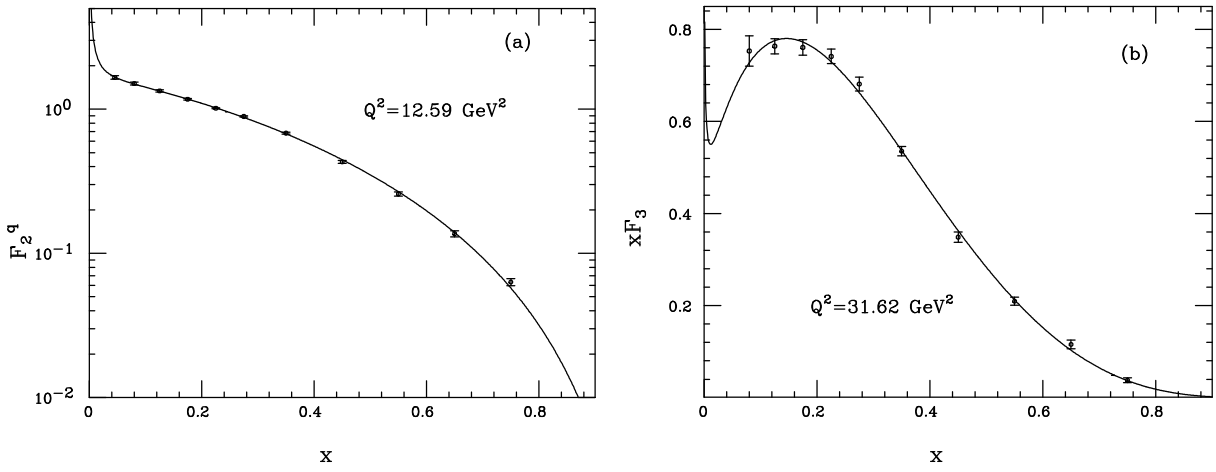

Fig. 2: NuTeV data on the quark-initiated contribution F_2^q to the structure function F_2, for $Q^2 = 12.59\ \mathrm{GeV}^2$ (a), and $Q^2 = 31.62\ \mathrm{GeV}^2$ (b). The solid lines are the best-fit predictions.

where C_i^q is the relevant coefficient function and q_i is a combination of quark and antiquark distributions only. Hereafter, we shall take $\mu = \mu_F = Q$ for the factorization and renormalization scales. At this point, to identify individual quark distributions from this limited set of data, we need to make some simplifying assumptions. Following [47], we assume isospin symmetry of the sea, $\bar{u} = \bar{d}$, $s = \bar{s}$ and we further impose a simple proportionality relation expressing the antistrange density in terms of the other antiquarks, $\bar{s} = \kappa\bar{u}$. As in [47], we shall present results for $\kappa = \frac{1}{2}$. With these assumptions, we can explicit solve for the remaining three independent quark densities (up, down, and, say, strange), using the three data sets we are considering.

Taking the Mellin moments of Eq. (11), the convolution becomes an ordinary product and we can extract NLO or NLL-resummed parton densities, according to whether we use NLO or NLL coefficient functions. More precisely,

$$\hat{q}_i^{\mathrm{NLO}}(N, Q^2) = \frac{\hat{F}_i(N-1, Q^2)}{\hat{C}_i^{\mathrm{NLO}}\left(N, 1, \alpha_s(Q^2)\right)} \ ; \quad \hat{q}_i^{\mathrm{res}}(N, Q^2) = \frac{\hat{F}_i(N-1, Q^2)}{\hat{C}_i^{\mathrm{res}}\left(N, 1, \alpha_s(Q^2)\right)} \ . \tag{12}$$

After extracting the combinations q_i, one can derive the individual quark densities, at NLO and including NLL large-x resummation. We concentrate our analysis on the up quark distribution, since experimental

errors on the structure functions are too large to see an effect of the resummation on the other quark densities, such as d or s, with the limited data set we are using.

2.3 Impact of the resummation

We present results for moments of the up quark distribution in Figs. 3 and 4. Resummation effects

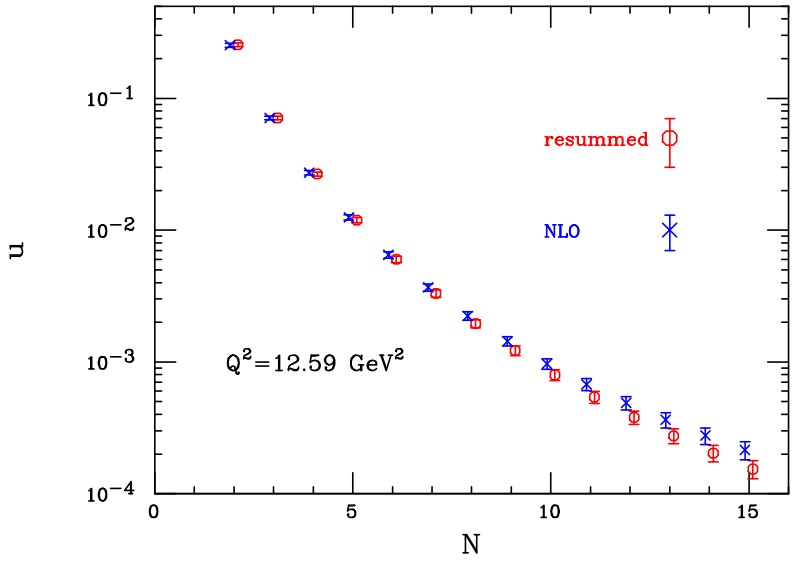

Fig. 3: NLO and resummed moments of the up quark distribution at $Q^2 = 12.59$ GeV^2

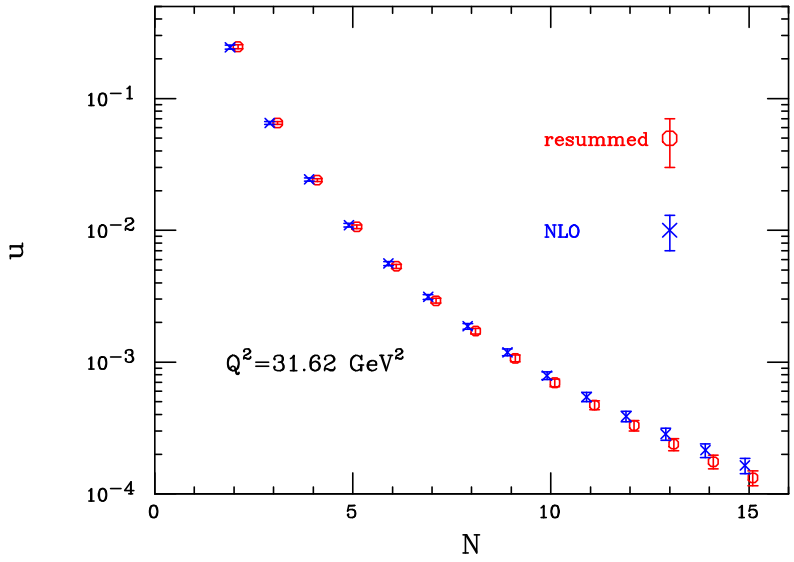

Fig. 4: As in Fig. 3, but at $Q^2 = 31.62$ GeV^2.

become statistically significant around $N \sim 6-7$ at both values of Q^2. Notice that high moments of the resummed up density are *suppressed* with respect to the NLO density, as a consequence of the fact that resummation in the $\overline{\rm MS}$ scheme enhances high moments of the coefficient functions.

In order to illustrate the effect in the more conventional setting of x-space distributions, we fit our results for the moments to a simple parametrization of the form $u(x) = Dx^{-\gamma}(1-x)^{\delta}$. Our best fit values for the parameters, with statistical errors, are given in Table (1), and the resulting distributions

Table 1: Best fit values and errors for the up-quark x-space parametrization, at the chosen values of Q^2.

Q^2	PDF	D	γ	δ
12.59	NLO	3.025 ± 0.534	0.418 ± 0.101	3.162 ± 0.116
	RES	4.647 ± 0.881	0.247 ± 0.109	3.614 ± 0.128
31.62	NLO	2.865 ± 0.420	0.463 ± 0.086	3.301 ± 0.098
	RES	3.794 ± 0.583	0.351 ± 0.090	3.598 ± 0.104

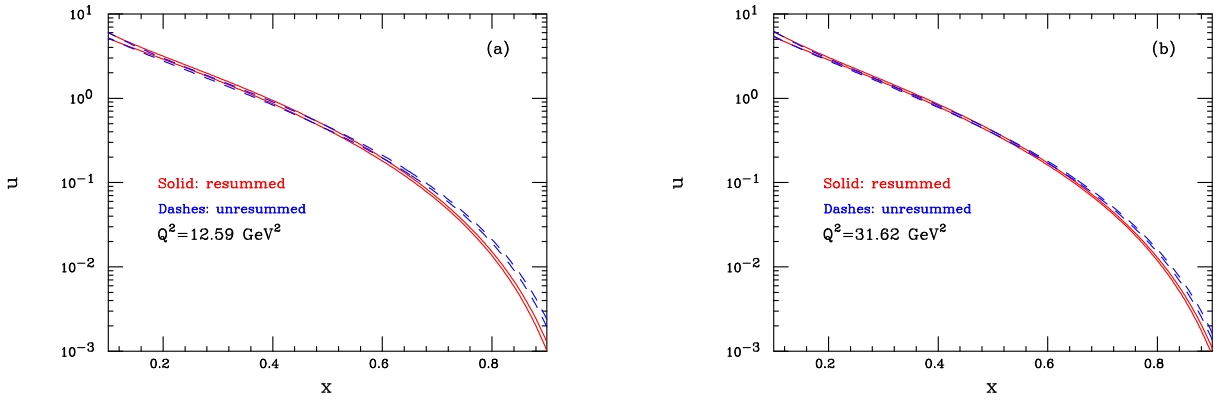

Fig. 5: NLO and resummed up quark distribution at $Q^2 = 12.59$ GeV^2 (a) and at $Q^2 = 31.62$ GeV^2, using the parametrization given in the text. The band corresponds to one standard deviation in parameter space.

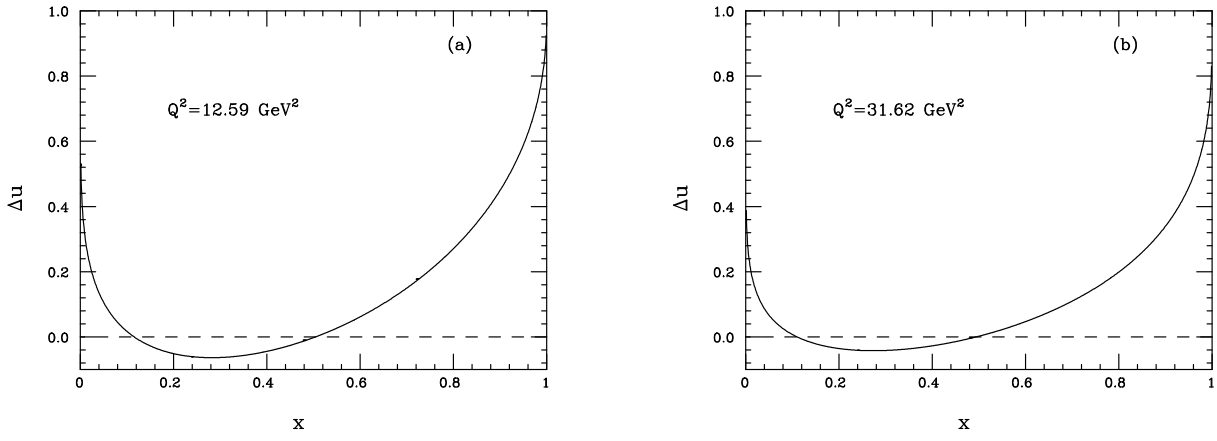

Fig. 6: Central value of relative change in the up quark distribution, $\Delta u(x) \equiv \left(u_{\rm NLO}(x) - u_{\rm res}(x)\right)/u_{\rm NLO}(x)$, at $Q^2 = 12.59$ (a) and 31.62 GeV^2 (b).

are displayed in Fig. 5, with one standard deviation uncertainty bands. Once again, the effect of soft resummation is clearly visible at large x: it suppresses the quark densities extracted from the given structure function data with respect to the NLO prediction.

In order to present the effect more clearly, we show in Fig. 6 the normalized deviation of the NLL-resummed prediction from the NLO one, i.e. $\Delta u(x) = \left(u_{\rm NLO}(x) - u_{\rm res}(x)\right)/u_{\rm NLO}(x)$, at the two chosen values of Q^2 and for the central values of the best-fit parameters. We note a change in the sign of Δu in the neighborhhod of the point $x = 1/2$: although our errors are too large for the effect to be statistically significant, it is natural that the suppression of the quark distribution at large x be

compensated by an enhancement at smaller x. In fact, the first moment of the coefficient function is unaffected by the resummation: thus C_i^q, being larger at large x, must become smaller at small x. The further sign change at $x \sim 0.1$, on the other hand, should not be taken too seriously, since our sample includes essentially no data at smaller x, and of course we are using an x-space parametrization of limited flexibility.

Finally, we wish to verify that the up-quark distributions extracted by our fits at $Q^2 = 12.59$ and 31.62 GeV^2 are consistent with perturbative evolution. To achieve this goal, we evolve our N-space results at $Q^2 = 31.62$ GeV^2 down to 12.59 GeV^2, using NLO Altarelli–Parisi anomalous dimensions, and compare the evolved moments with the direct fit at 12.59 GeV^2. Figures 7 and 8 show that the results of our fits at 12.59 GeV^2 are compatible with the NLO evolution within the confidence level of one standard deviation. Note however that the evolution of resummed moments appears to give less consistent results, albeit within error bands: this can probably be ascribed to a contamination between pertubative resummation and power corrections, which we have not disentangled in our analysis.

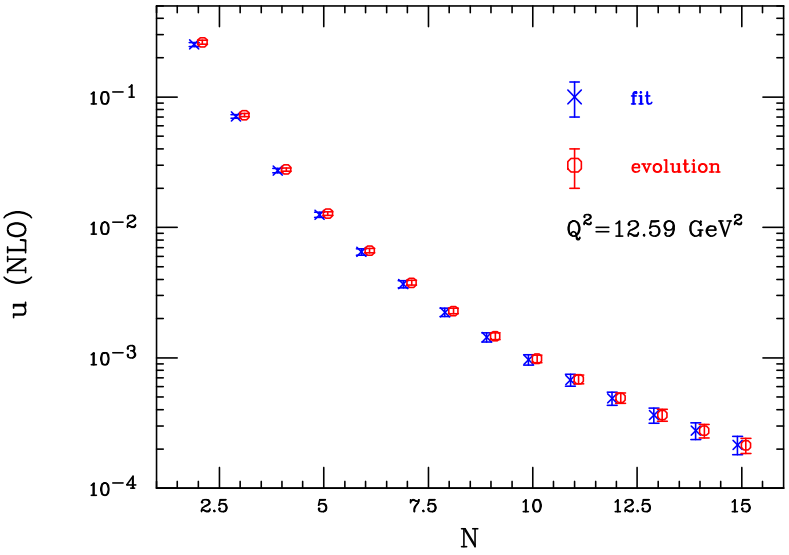

Fig. 7: Comparison of fitted moments of the NLO up quark distribution, at $Q^2 = 12.59$ GeV^2, with moments obtained via NLO evolution from $Q^2 = 31.62$ GeV^2.

Qualitatively, the observed effect on the up quark distribution is easily described, at least within the limits of a simple parametrization like the one we are employing: resummation increases the exponent δ, responsible for the power-law decay of the distribution at large x, by about 10% to 15% at moderate Q^2. The exponent γ, governing the small-x behavior, and the normalization D, are then tuned so that the first finite moment (the momentum sum rule) may remain essentially unaffected.

In conclusion, our results indicate that quark distributions are suppressed at large x by soft gluon effects. Quantitatively, we observe an effect ranging between 10% and 20% when $0.6 < x < 0.8$ at moderate Q^2, where we expect power corrections not to play a significant role. Clearly, a more detailed quantitative understanding of the effect can be achieved only in the context of a broader and fully consistent fit. We would like however to notice two things: first, the effect of resummations propagates to smaller values of x, through the fact that the momentum sum rule is essentially unaffected by the resummation; similarly, evolution to larger values of Q^2 will shift the Sudakov suppression to smaller x. A second point is that, in a fully consistent treatment of hadronic cross section, there might be a partial compensation between the typical Sudakov enhancement of the partonic process and the Sudakov suppression of the quark distribution: the compensation would, however, be channel-dependent, since gluon-initiated partonic processes would be unaffected. We believe it would be interesting, and phenomenologically relevant, to investigate these issues in the context of a more comprehensive parton fit.

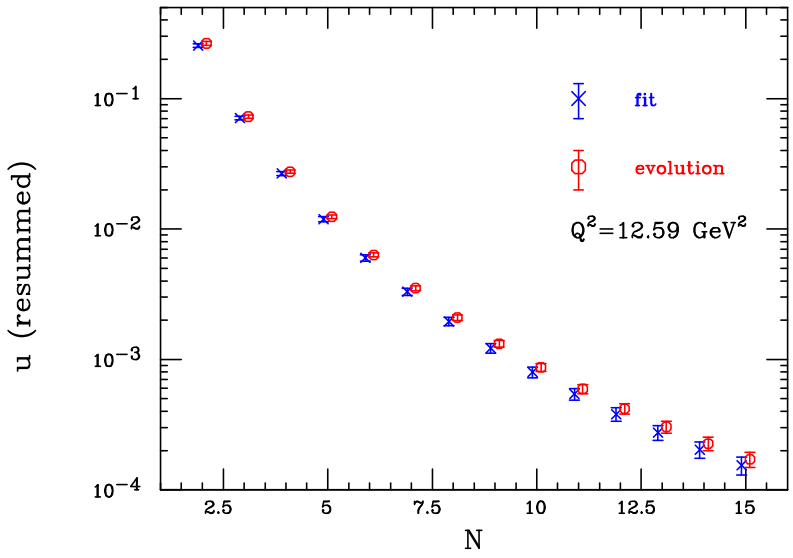

Fig. 8: As in Fig. 7, but comparing NLL-resummed moments of the up quark density.

3 Small x

Small x structure functions are dominated by the flavour singlet contribution, whose coefficient functions and anomalous dimensions receive logarithmic enhancements, which make perturbation theory converge more slowly. In the small x, i.e. high energy limit, the cross section is quasi-constant and characterised by the effective expansion parameter $\langle\alpha_s(\boldsymbol{k}^2)\rangle \log\frac{1}{x}\log\frac{\boldsymbol{k}^2_{\max}}{\boldsymbol{k}^2_{\min}}$, where $x = Q^2/s$, $\boldsymbol{k}^2 \lesssim Q^2$ is the transverse momentum of the exchanged gluon, s is the photon-proton centre of mass energy squared and Q^2 is the hard scale. Such expansion parameter can be large, due to both the double-logs and to the fact that $\langle\boldsymbol{k}^2\rangle$ may drift towards the non-perturbative region. Even assuming that truly non-perturbative effects are factored out — as is the case for structure functions — the problem remains of resumming the perturbative series with both kinds of logarithms [11–17]

In the BFKL approach one tries to resum the high-energy logarithms first, by an evolution equation in $\log 1/x$, whose $\boldsymbol{k}$-dependent evolution kernel is calculated perturbatively in α_s. However, the leading kernel [14–17] overestimates the hard cross-section, and subleading ones [19, 20, 49] turn out to be large and of alternating sign, pointing towards an instability of the leading-$\log x$ (Lx) hierarchy. The problem is that, for any given value of the hard scales $Q, Q_0 \ll \sqrt{s}$ — think, for definiteness, of $\gamma^*(Q)$-$\gamma^*(Q_0)$ collisions —, the contributing kernels contain collinear enhancements in all $\boldsymbol{k}$-orderings of the exchanged gluons of type $\sqrt{s} \gg \cdots \boldsymbol{k}_1 \gg \boldsymbol{k}_2 \cdots$, or $\sqrt{s} \gg \cdots \boldsymbol{k}_2 \gg \boldsymbol{k}_1 \cdots$ and so on, to all orders in α_s. Such enhancements are only partly taken into account by any given truncation of the Lx hierarchy, and they make it unstable. In the DGLAP evolution equation one resums collinear logarithms first, but fixed order splitting functions do contain [6, 18] high-energy logarithms also, and a further resummation is needed.

Two approaches to the simultaneous resummation of these two classes of logs have recently reached the stage where their phenomenological application can be envisaged. The renormalisation group improved (CCSS) approach [21–23, 50] is built up within the BFKL framework, by improving the whole hierarchy of subleading kernels in the collinear region, so as to take into account all the $\boldsymbol{k}$-orderings mentioned before, consistently with the RG. In the duality (ABF) approach [24–30, 51] one concentrates on the problem of obtaining an improved anomalous dimension (splitting function) for DIS which reduces to the ordinary perturbative result at large N (large x), thereby automatically satisfying renormalization group constraints, while including resummed BFKL corrections at small N (small x), determined through the renormalization-group improved (i.e. running coupling) version of the BFKL kernel.

We will briefly review the theoretical underpinnings of these two approaches in turn, and then compare phenomenological results obtained in both approaches. Note that we shall use the notation of the CCSS or ABF papers in the corresponding sections, in order to enable a simpler connection with the original literature, at the price of some notational discontinuity. In particular, $\ln \frac{1}{x}$ is called Y by CCSS and ξ by ABF; the Mellin variable conjugate to $\ln \frac{1}{x}$ is called ω by CCSS and N by ABF; and the Mellin variable conjugated to $\ln \frac{Q^2}{\boldsymbol{k}^2}$ is called γ by CCSS and M by ABF.

3.1 The renormalisation group improved approach

The basic problem which is tackled in the CCSS approach [21–23, 50] is the calculation of the (azimuthally averaged) gluon Green function $\mathcal{G}(Y; k, k_0)$ as a function of the magnitudes of the external gluon transverse momenta $k \equiv |\boldsymbol{k}|,\ k_0 \equiv |\boldsymbol{k}_0|$ and of the rapidity $Y \equiv \log \frac{s}{kk_0}$. This is not yet a hard cross section, because one needs to incorporate the impact factors of the probes [52–59]. Nevertheless, the Green function exhibits most of the physical features of the hard process, if we think of $k^2,\ k_0^2$ as external (hard) scales. The limits $k^2 \gg k_0^2$ ($k_0^2 \gg k^2$) correspond conventionally to the ordered (anti-ordered) collinear limit. By definition, in the ω-space conjugate to Y (so that $\hat{\omega} = \partial_Y$) one sets

$$\mathcal{G}_\omega(\boldsymbol{k}, \boldsymbol{k}_0) \equiv [\omega - \mathcal{K}_\omega]^{-1}(\boldsymbol{k}, \boldsymbol{k}_0)\,, \tag{13}$$

$$\omega \mathcal{G}_\omega(\boldsymbol{k}, \boldsymbol{k}_0) = \delta^2(\boldsymbol{k} - \boldsymbol{k}_0) + \int d^2\boldsymbol{k}'\ \mathcal{K}_\omega(\boldsymbol{k}, \boldsymbol{k}')\mathcal{G}_\omega(\boldsymbol{k}', \boldsymbol{k}_0)\ , \tag{14}$$

where $\mathcal{K}_\omega(\boldsymbol{k}, \boldsymbol{k}')$ is a kernel to be defined, whose $\omega = 0$ limit is related to the BFKL Y-evolution kernel discussed before.

In order to understand the RG constraints, it is useful to switch from $\boldsymbol{k}$-space to γ-space, where the variable γ is conjugated to $t \equiv \log \boldsymbol{k}^2/\boldsymbol{k}_0^2$ at fixed Y, and to make the following kinematical remark: the ordered (anti-ordered) region builds up scaling violations in the Bjorken variable $x = \boldsymbol{k}^2/s$ ($x_0 = \boldsymbol{k}_0^2/s$) and, if x (x_0) is fixed instead of $kk_0/s = e^{-Y}$, the variable conjugated to t is shifted [60] by an ω-dependent amount, and becomes $\gamma + \frac{\omega}{2} \sim \partial_{\log \boldsymbol{k}^2}$ ($1 - \gamma + \frac{\omega}{2} \sim \partial_{\log \boldsymbol{k}_0^2}$). Therefore, the characteristic function $\chi_\omega(\gamma)$ of $\mathcal{K}_\omega$ (with a factor α_s factored out) must be singular when either one of the variables is small, as shown (in the frozen α_s limit) by

$$\frac{1}{\omega}\chi_\omega(\gamma) \to \left[\frac{1}{\gamma + \frac{\omega}{2}} + \frac{1}{1 - \gamma + \frac{\omega}{2}} + \cdots\right]\left[\gamma_{gg}^{(1)}(\alpha_s, \omega) + \cdots\right]\ , \tag{15}$$

where $\gamma_{gg}^{(1)}$ is the one-loop gluon anomalous dimension, and further orders may be added. Eq. (15) ensures the correct DGLAP evolution in either one of the collinear limits (because, e.g., $\gamma + \frac{\omega}{2} \sim \partial_{\log \boldsymbol{k}^2}$) and is ω-dependent, because of the shifts. Since higher powers of ω are related to higher subleading powers of α_s [61], this ω-dependence of the constraint (15) means that the whole hierarchy of subleading kernels is affected.

To sum up, the kernel $\mathcal{K}_\omega$ is constructed so as to satisfy the RG constraint (15) and to reduce to the exact Lx + NLx BFKL kernels in the $\omega \to 0$ limit; it is otherwise interpolated on the basis of various criteria (e.g., momentum conservation), which involve a "scheme" choice.

The resulting integral equation has been solved in [21–23] by numerical matrix evolution methods in $\boldsymbol{k}$- and x-space. Furthermore, introducing the integrated gluon density g, the resummed splitting function $P_{\text{eff}}(x, Q^2)$ is defined by the evolution equation

$$\frac{\partial g(x, Q^2)}{\partial \log Q^2} = \int \frac{\mathrm{d}z}{z}\ P_{\text{eff}}\big(z, \alpha_s(Q^2)\big) g\Big(\frac{x}{z}, Q^2\Big)\ , \tag{16}$$

and has been extracted [21–23] by a numerical deconvolution method [62]. Note that in the RGI approach the running of the coupling is treated by adopting in (14) the off-shell dependence of α_s suggested by the BFKL and DGLAP limits, and then solving the ensuing integral equation numerically.

It should be noted that the RGI approach has the somewhat wider goal of calculating the off-shell gluon density (13), not only its splitting function. Therefore, a comparison with the ABF approach, to be discussed below, is possible in the "on-shell" limit, in which the homogeneous (eigenvalue) equation of RGI holds. In the frozen coupling limit we have simply

$$\chi_\omega(\alpha_s, \gamma - \tfrac{\omega}{2}) = \omega \ , \qquad (\chi_\omega \text{ is at scale } kk_0) \ . \tag{17}$$

In the same spirit as the ABF approach [24–30, 51], when solving Eq. (17) for either ω or γ, we are able to identify the effective characteristic function and its dual anomalous dimension

$$\omega = \chi_{\rm eff}(\alpha_s, \gamma) \ ; \quad \gamma = \gamma_{\rm eff}(\alpha_s, \omega) \ . \tag{18}$$

3.2 The duality approach

As already mentioned, in the ABF approach one constructs an improved anomalous dimension (splitting function) for DIS which reduces to the ordinary perturbative result at large N (large x) given by:

$$\gamma(N, \alpha_s) = \alpha_s \gamma_0(N) \ + \ \alpha_s^2 \gamma_1(N) \ + \ \alpha_s^3 \gamma_2(N) \ \ \ldots . \tag{19}$$

while including resummed BFKL corrections at small N (small x) which are determined by the aforementioned BFKL kernel $\chi(M, \alpha_s)$:

$$\chi(M, \alpha_s) = \alpha_s \chi_0(M) \ + \ \alpha_s^2 \chi_1(M) \ + \ \ldots , \tag{20}$$

which is the Mellin transform of the $\omega \to 0$, angular averaged kernel $\mathcal{K}$ eq. 14 with respect to $t = \ln \frac{k^2}{k_0^2}$. The main theoretical tool which enables this construction is the duality relation between the kernels χ and γ [compare Eq. (18)]

$$\chi(\gamma(N, \alpha_s), \alpha_s) = N, \tag{21}$$

which is a consequence of the fact that the solutions of the BFKL and DGLAP equations coincide at leading twist [24, 51, 63]. Further improvements are obtained exploiting the symmetry under gluon interchange of the BFKL gluon-gluon kernel and through the inclusion of running coupling effects.

By using duality, one can construct a more balanced expansion for both γ and χ, the "double leading" (DL) expansion, where the information from χ is used to include in γ all powers of α_s/N and, conversely γ is used to improve χ by all powers of α_s/M. A great advantage of the DL expansion is that it resums the collinear poles of χ at $M = 0$, enabling the imposition of the physical requirement of momentum conservation $\gamma(1, \alpha_s) = 0$, whence, by duality:

$$\chi(0, \alpha_s) = 1. \tag{22}$$

This procedure eliminates in a model independent way the alternating sign poles $+1/M, -1/M^2, ...$ that appear in χ_0, χ_1,.... These poles make the perturbative expansion of χ unreliable even in the central region of M: e.g., $\alpha_s\chi_0$ has a minimum at $M = 1/2$, while, at realistic values of α_s, $\alpha_s\chi_0 + \alpha_s^2\chi_1$ has a maximum.

At this stage, while the poles at $M = 0$ are eliminated, those at $M = 1$ remain, so that the DL expansion is still not finite near $M = 1$. The resummation of the $M = 1$ poles can be accomplished by exploiting the collinear-anticollinear symmetry, as suggested in the CCSS approach discussed above. In Mellin space, this symmetry implies that at the fixed-coupling level the kernel χ for evolution in $\ln \frac{s}{kk_0}$ must satisfy $\chi(M) = \chi(1 - M)$. This symmetry is however broken by the DIS choice of variables $\ln \frac{1}{x} = \ln \frac{s}{Q^2}$ and by the running of the coupling. In the fixed coupling limit the kernel $\chi_{\rm DIS}$, dual to the DIS anomalous dimension, is related to the symmetric one χ_σ through the implicit equation [49]

$$\chi_{\rm DIS}(M + 1/2\chi_\sigma(M)) = \chi_\sigma(M), \tag{23}$$

to be compared to eq. (17) of the CCSS approach.

Hence, the $M = 1$ poles can be resummed by performing the double-leading resummation of $M = 0$ poles of $\chi_{\rm DIS}$, determining the associated χ_σ through eq. (23), then symmetrizing it, and finally going back to DIS variables by using eq. (23) again in reverse. Using the momentum conservation eq. (22) and eq. (23), it is easy to show that $\chi_\sigma(M)$ is an entire function of M, with $\chi_\sigma(-1/2) = \chi_\sigma(3/2) = 1$ and has a minimum at $M = 1/2$. Through this procedure one obtains order by order from the DL expansion a symmetrized DL kernel $\chi_{\rm DIS}$, and its corresponding dual anomalous dimension γ. The kernel $\chi_{\rm DIS}$ has to all orders a minimum and satisfies a momentum conservation constraint $\chi_{\rm DIS}(0) = \chi_{\rm DIS}(2) = 1$.

The final ingredient of the ABF approach is a treatment of the running coupling corrections to the resummed terms. Indeed, their inclusion in the resummed anomalous dimension greatly softens the asymptotic behavior near $x = 0$. Hence, the dramatic rise of structure functions at small x, which characterized resummations based on leading–order BFKL evolution, and is ruled out phenomenologically, is replaced by a much milder rise. This requires a running coupling generalization of the duality Eq. (21), which is possible noting that in M space the running coupling $\alpha_s(t)$ becomes a differential operator, since $t \to d/dM$. Hence, the BFKL evolution equation for double moments $G(N, M)$, which is an algebraic equation at fixed coupling, becomes a differential equation in M for running coupling. In the ABF approach, one solves this differential equation analytically when the kernel is replaced by its quadratic approximation near the minimum. The solution is expressed in terms of an Airy function if the kernel is linear in α_s, for example in the case of $\alpha_s\chi_0$, or of a Bateman function in the more general case of a non linear dependence on α_s as is the case for the DL kernels. The final result for the improved anomalous dimension is given in terms of the DL expansion plus the "Airy" or "Bateman" anomalous dimension, with the terms already included in the DL expansion subtracted away.

For example, at leading DL order, i.e. only using $\gamma_0(N)$ and $\chi_0(M)$, the improved anomalous dimension is

$$\gamma_I^{NL}(\alpha_s, N) = \left[\alpha_s\gamma_0(N) + \alpha_s^2\gamma_1(N) + \gamma_s(\frac{\alpha_s}{N}) - \frac{n_c\alpha_s}{\pi N}\right] + \gamma_A(c_0, \alpha_s, N) - \frac{1}{2} + \sqrt{\frac{2}{\kappa_0\alpha_s}[N - \alpha_s c_0]}. \tag{24}$$

The terms within square brackets give the LO DL approximation, i.e. they contain the fixed–coupling information from γ_0 and (through γ_s) from χ_0. The "Airy" anomalous dimension $\gamma_A(c_0, \alpha_s, N)$ contains the running coupling resummation, i.e. it is the exact solution of the running coupling BFKL equation which corresponds to a quadratic approximation to χ_0 near $M = 1/2$. The last two terms subtract the contributions to $\gamma_A(c_0, \alpha_s, N)$ which are already included in γ_s and γ_0. In the limit $\alpha_s \to 0$ with N fixed, $\gamma_I(\alpha_s, N)$ reduces to $\alpha_s\gamma_0(N) + O(\alpha_s^2)$. For $\alpha_s \to 0$ with α_s/N fixed, $\gamma_I(\alpha_s, N)$ reduces to $\gamma_s(\frac{\alpha_s}{N}) + O(\alpha_s^2/N)$, i.e. the leading term of the small x expansion. Thus the Airy term is subleading in both limits. However, if $N \to 0$ at fixed α_s, the Airy term replaces the leading singularity of the DL anomalous dimension, which is a square root branch cut, with a simple pole, located on the real axis at rather smaller N, thereby softening the small x behaviour. The quadratic approximation is sufficient to give the correct asymptotic behaviour up to terms which are of subleading order in comparison to those included in the DL expression in eq. (24).

The running coupling resummation procedure can be applied to a symmetrized kernel, which possesses a minimum to all orders, and then extended to next-to-leading order [29, 30]. This entails various technical complications, specifically related to the nonlinear dependence of the symmetrized kernel on α_s, to the need to include interference between running coupling effects and the small x resummation, and to the consistent treatment of next-to-leading log Q^2 terms, in particular those related to the running of the coupling. It should be noted that even though the ABF appraoch is limited to the description of leading-twist evolution at zero-momentum transfer, it leads to a pair of systematic dual perturbative expansions for the χ and γ kernels. Hence, comparison with the CCSS approach is possible for instance by comparing the NLO ABF kernel to the RG improved Lx+NLx CCSS kernel.

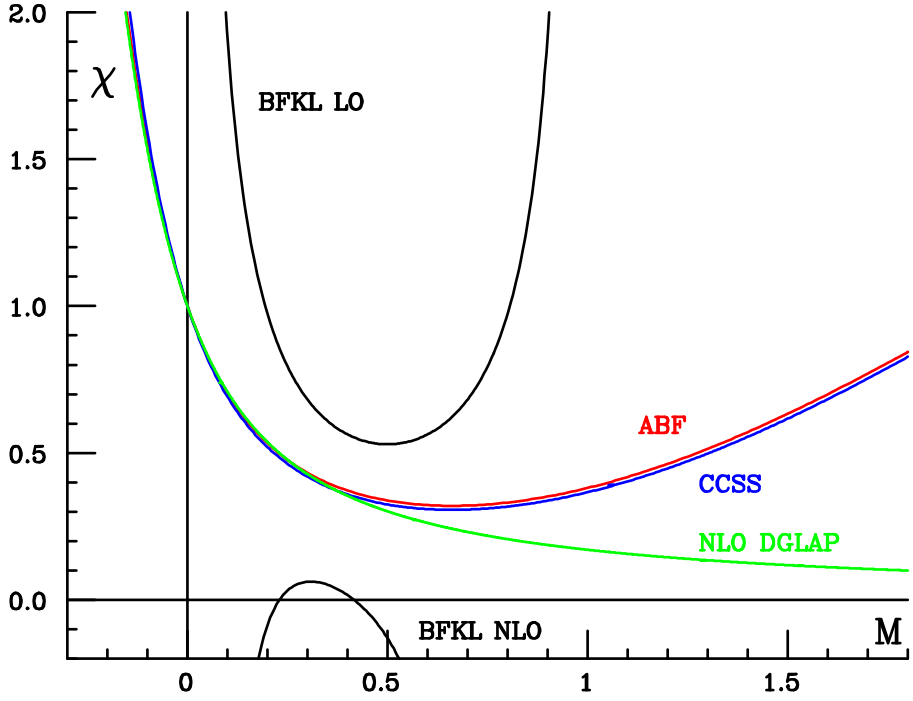

Fig. 9: The kernel χ (BFKL characteristic function) for fixed coupling ($\beta_0 = 0$) $\alpha_s = 0.2$ and $n_f = 0$. The BFKL curves are the LO and NLO truncations of eq. (20), the DGLAP curve is the dual eq. (21) of the NLO anomalous dimension eq. (19), while the CCSS and ABF curves are respectively the solution ω of eq. (17) and the solution $\chi_{\rm DIS}$ of eq. (23).

3.3 Comparison of results

Even though the basic underlying physical principles of the CCSS and ABF approaches are close, there are technical differences in the construction of the resummed RG-improved (CCSS) or symmetrized DL (ABF) kernel, in the derivation from it of an anomalous dimension and associated splitting function, and in the inclusion of running coupling effects. Therefore, we will compare results for the resummed fixed-coupling χ kernel (BFKL characteristic function), then the corresponding fixed-coupling splitting functions, and finally the running coupling splitting functions which provide the final result in both approaches. In order to assess the phenomenological impact on parton evolution we will finally compare the convolution of the splitting function with a "typical" gluon distribution.

In Fig. 9 we compare the solution, ω, to the on-shell constraint, eq. (17) for the RGI CCSS result, and the solution $\chi_{\rm DIS}$ of eq. (23) for the symmetrized NLO DL ABF result. The pure Lx and NLx (BFKL) and next-to-leading $\ln Q^2$ (DGLAP) are also shown. All curves are determined with frozen coupling ($\beta_0 = 0$), and with $n_f = 0$, in order to avoid complications related to the diagonalization of the DGLAP anomalous dimension matrix and to the choice of scheme for the quark parton distribution. The resummed CCSS and ABF results are very close, in that they coincide by construction at the momentum conservation points $M = \frac{1}{2}$ and $M = 2$, and differ only in the treatment of NLO DGLAP terms. In comparison to DGLAP, the resummed kernels have a minimum, related to the fact that both collinear and anticollinear logs are resummed. In comparison to BFKL, which has a minimum at LO but not NLO, the resummed kernels always have a perturbatively stable minimum, characterized by a lower intercept than leading–order BFKL: specifically, when $\alpha_s = 0.2$, $\lambda \sim 0.3$ instead of $\lambda \sim 0.5$. This corresponds to a softer small x rise of the associated splitting function.

The fixed–coupling resummed splitting functions up to NLO are shown in figure 10, along with

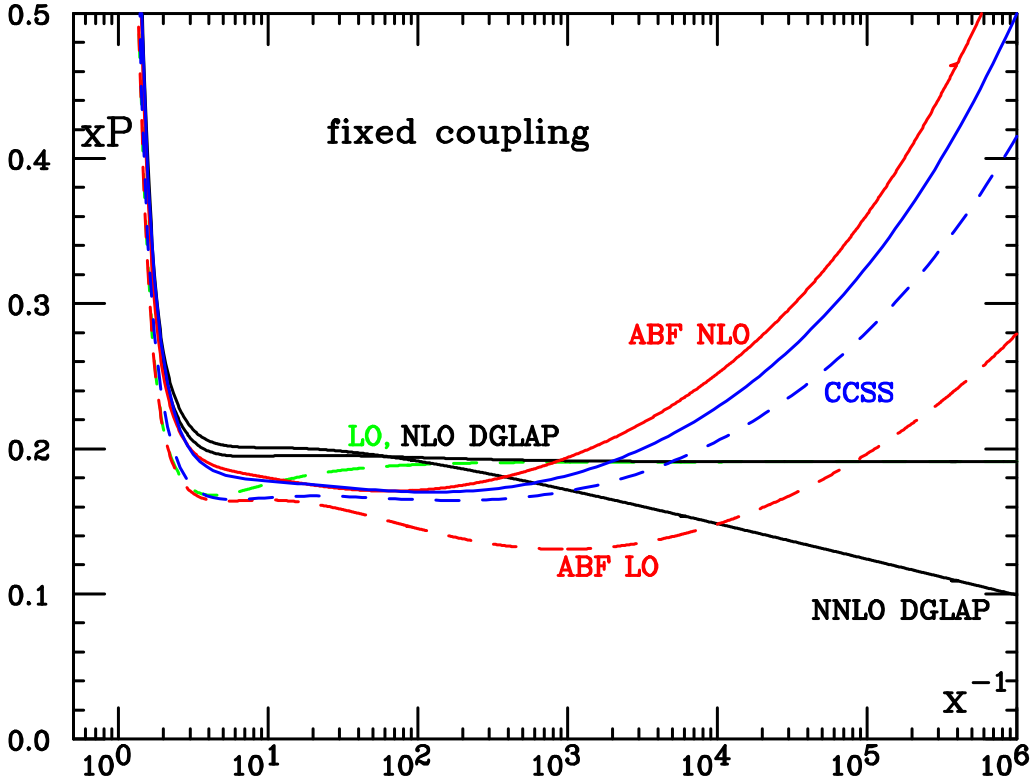

Fig. 10: The fixed coupling ($\beta_0 = 0$) $xP_{gg}(x)$ splitting function, evaluated with $\alpha_s = 0.2$ and $n_f = 0$. The dashed curves are LO for DGLAP, NLx+LO for CCSS and symmetrized LO DL for ABF, while the solid curves are NLO and NNLO for DGLAP, NLx+NLO for CCSS and symmetrized NLO DL for ABF.

the unresummed DGLAP splitting functions up to NNLO.[2] In the CCSS approach the splitting function is determined by explicitly solving eq. (14) with the kernel corresponding to figure 9, and then applying the numerical deconvolution procedure of [62]. For $n_f = 0$ the NLO DGLAP splitting function has the property that it vanishes at small x — this makes it relatively straightforward to combine not just LO DGLAP but also NLO DGLAP with the NLLx resummation. Both the CCSS NLx+LO and NLx+NLO curves are shown in Fig. 10. On the other hand, in the ABF approach the splitting function is the inverse Mellin transform of the anomalous dimension obtained using duality Eq. (21) from the symmetrized DL χ kernel. Hence, the LO and NLO resummed result respectively reproduce all information contained in the LO and NLO χ and γ kernel with the additional constraint of collinear-anticollinear symmetry. Both the ABF LO and NLO results are shown in figure 10.

In comparison to unresummed results, the resummed splitting functions display the characteristic rise at small x of fixed-coupling leading-order BFKL resummation, though the small x rise is rather milder ($\sim x^{-0.3}$ instead of $\sim x^{-0.5}$ for $\alpha_s = 0.2$). At large x there is good agreement between the resummed results and the corresponding LO (dashed) or NLO (solid) DGLAP curves. At small x the difference between the ABF LO and CCSS NLx+LO (dashed) curves is mostly due to the inclusion in CCSS of BFKL NLx terms, as well as to differences in the symmetrization procedure. When comparing CCSS NLx+NLO with ABF NLO this difference is reduced, and , being only due the way the symmetrization is implemented, it might be taken as an estimate of the intrinsic ambiguity of the fixed–coupling resummation procedure. At intermediate x the NLO resummed splitting functions is of a similar order of magnitude as the NLO DGLAP result even down to quite small x, but with a somewhat different

[2] Starting from NLO one needs also to specify a factorisation scheme. Small-x results are most straightforwardly obtained in the Q_0 scheme, while fixed-order splitting functions are quoted in the $\overline{\rm MS}$ scheme (for discussions of the relations between different schemes see [25, 50, 64, 65]).

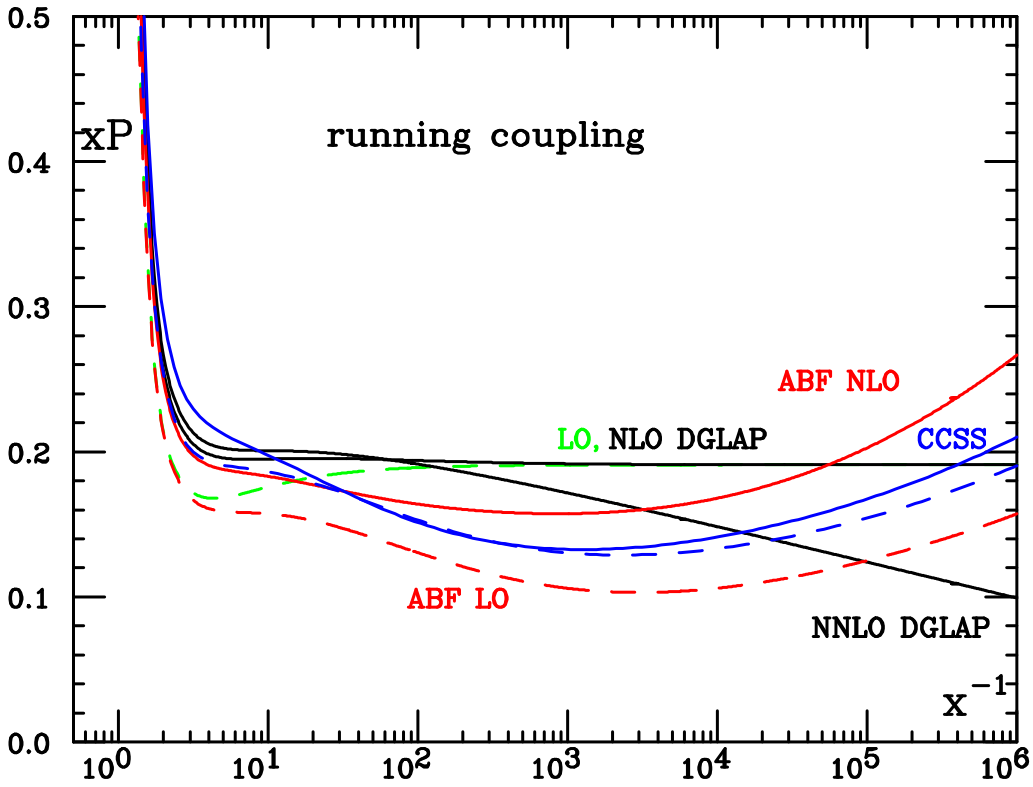

Fig. 11: The running coupling $xP_{gg}(x)$ splitting function, evaluated with $\alpha_s = 0.2$ and $n_f = 0$. The various curves correspond to the same cases as in figure 10.

shape, characterized by a shallow dip at $x \sim 10^{-2}$, until the small x rise sets in for $x \sim 10^{-3}$. It has been suggested [66] that in the small α_s limit this dip can be explained as a consequence of the interplay between the $-{\alpha_s}^3 \ln x$ NNLO term of xP_{gg} (also present in the resummation) and the first positive resummation effects which start with an ${\alpha_s}^4 \ln^3 1/x$ term. The unstable small x drop of the NNLO DGLAP result appears to be a consequence of the unresummed $\frac{\alpha_s^3}{N^2}$ double pole in the NNLO anomalous dimension.

The running-coupling resummed splitting functions are displayed in figure 11. Note that the unresummed curves are the same as in the fixed coupling case since their dependence on α_s is just through a prefactor of α_s^k, whereas in the resummed case there is an interplay between the running of the coupling and the structure of the small-x logs. All the resummed curves display a considerable softening of the small x behaviour in comparison to their fixed-coupling counterparts, due to the softening of the leading small x singularity in the running-coupling case [21, 26]. As a consequence, the various resummed results are closer to each other than in the fixed-coupling case, and also closer to the unresummed LO and NLO DGLAP results. The resummed perturbative expansion appears to be stable, subject to moderate theoretical ambiguity, and qualitatively close to NLO DGLAP.

Finally, to appreciate the impact of resummation it is useful to investigate not only the properties of the splitting function, but also its convolution with a physically reasonable gluon distribution. We take the following toy gluon

$$xg(x) = x^{-0.18}(1-x)^5\,, \tag{25}$$

and show in Fig. 12 the result of its convolution with various splitting functions of Fig. 11. The differences between resummed and unresummed results, and between the CCSS and ABF resummations are partly washed out by the convolution, even though the difference between the unresummed LO and NLO DGLAP results is clearly visible. In particular, differences between the fixed-order and resummed

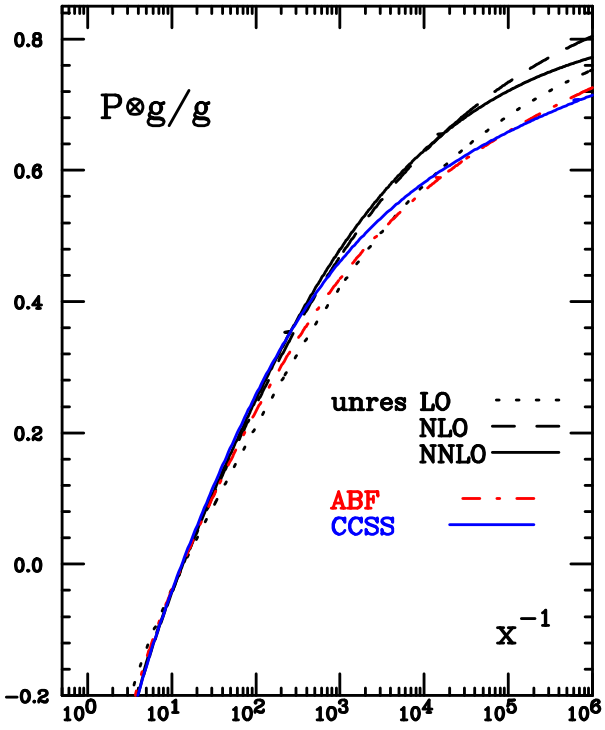

Fig. 12: Convolution of resummed and fixed-order P_{gg} splitting functions with a toy gluon distribution, Eq. (25), normalised to the gluon distribution itself, with $\alpha_s = 0.2$ and $n_f = 0$. The resummed CCSS and ABF curves are obtained using respectively the CCSS NLx+NLO and the ABF NLO splitting function shown in Fig. 11.

convolution start to become significant only for $x \lesssim 10^{-2} - 10^{-3}$, even though resummation effects started to be visible in the splitting functions at somewhat larger x.

It should be kept in mind that it is only the gg entry of the singlet splitting function matrix that has so far been investigated at this level of detail and that the other entries may yet reserve surprises.

3.4 Explicit solution of the BFKL equation by Regge exponentiation

The CCSS approach of section 3.1 exploits a numerical solution of the BFKL equation in which the gluon Green's function is represented on a grid in x and k. This method provides an efficient determination of the azimuthally averaged Green's function and splitting functions — for percent accuracy, up to $Y = 30$, it runs in a few seconds — for a wide range of physics choices, e.g. pure NLx, various NLx+NLO schemes. Here we will discuss an alternative framework suitable to solve numerically the NLL BFKL integral equation [67], based on Monte Carlo generation of events, which can also be applied to the study of different resummation schemes and DIS, but so far has been investigated for simpler NLL BFKL kernels and Regge–like configurations. This method has the advantage that it automatically provides information about azimuthal decorrelations as well as the pattern of final-state emissions.

This appproach relies on the fact that, as shown in Ref. [67], it is possible to trade the simple and double poles in ϵ, present in $D = 4 + 2\epsilon$ dimensional regularisation, by a logarithmic dependence on an effective gluon mass λ. This λ dependence numerically cancels out when the full NLL BFKL evolution is taken into account for a given center–of–mass energy, a consequence of the infrared finiteness of the full kernel. The introduction of this mass scale, differently to the original work of Ref. [49] was performed without angular averaging the NLL kernel.

With such reguralisation of the infrared divergencies it is then convenient to iterate the NLL BFKL equation for the t–channel partial wave, generating, in this way, multiple poles in the complex ω–plane.

The positions of these singularities are set at different values of the gluon Regge trajectory depending on the transverse momenta of the Reggeized gluons entering the emission vertices. At this point it is possible to Mellin transform back to energy space and obtain an iterated form for the solution of the NLL BFKL equation:

$$
\begin{aligned}
f(\mathbf{k}_a,\mathbf{k}_b,\mathrm{Y}) &= e^{\omega_0^\lambda(\mathbf{k}_a)\mathrm{Y}}\,\delta^{(2)}(\mathbf{k}_a-\mathbf{k}_b) \\
&+\sum_{n=1}^{\infty}\prod_{i=1}^{n}\int d^2\mathbf{k}_i\int_0^{y_{i-1}} dy_i\left[\frac{\theta\left(\mathbf{k}_i^2-\lambda^2\right)}{\pi\mathbf{k}_i^2}\xi\left(\mathbf{k}_i\right)+\widetilde{\mathcal{K}}_r\left(\mathbf{k}_a+\sum_{l=0}^{i-1}\mathbf{k}_l,\mathbf{k}_a+\sum_{l=1}^{i}\mathbf{k}_l\right)\right] \\
&\times e^{\omega_0^\lambda\left(\mathbf{k}_a+\sum_{l=1}^{i-1}\mathbf{k}_l\right)(y_{i-1}-y_i)}\;e^{\omega_0^\lambda\left(\mathbf{k}_a+\sum_{l=1}^{i}\mathbf{k}_l\right)y_n}\delta^{(2)}\left(\sum_{l=1}^{n}\mathbf{k}_l+\mathbf{k}_a-\mathbf{k}_b\right),
\end{aligned}
\tag{26}
$$

where the strong ordering in longitudinal components of the parton emission is encoded in the nested integrals in rapidity with an upper limit set by the logarithm of the total energy in the process, $y_0=\mathrm{Y}$. The first term in the expansion corresponds to two Reggeized gluons propagating in the t–channel with no additional emissions. The exponentials carry the dependence on the Regge gluon trajectory, *i.e.*

$$
\omega_0^\lambda\left(\mathbf{q}\right) = -\bar{\alpha}_s\ln\frac{\mathbf{q}^2}{\lambda^2}+\frac{\bar{\alpha}_s^2}{4}\left[\frac{\beta_0}{2N_c}\ln\frac{\mathbf{q}^2}{\lambda^2}\ln\frac{\mathbf{q}^2\lambda^2}{\mu^4}+\left(\frac{\pi^2}{3}-\frac{4}{3}-\frac{5}{3}\frac{\beta_0}{N_c}\right)\ln\frac{\mathbf{q}^2}{\lambda^2}+6\zeta(3)\right], \tag{27}
$$

corresponding to no–emission probabilities between two consecutive effective vertices. Meanwhile, the real emission is built out of two parts, the first one:

$$
\xi\left(\mathrm{X}\right) \equiv \bar{\alpha}_s+\frac{\bar{\alpha}_s^2}{4}\left(\frac{4}{3}-\frac{\pi^2}{3}+\frac{5}{3}\frac{\beta_0}{N_c}-\frac{\beta_0}{N_c}\ln\frac{\mathrm{X}}{\mu^2}\right), \tag{28}
$$

which cancels the singularities present in the trajectory order by order in perturbation theory, and the second one: $\tilde{\mathcal{K}}_r$, which, although more complicated in structure, does not generate ϵ singularities when integrated over the full phase space of the emissions, for details see Ref. [67].

The numerical implementation and analysis of the solution as in Eq. (26) was performed in Ref. [68]. As in previous studies the intercept at NLL was proved to be lower than at leading–logarithmic (LL) accuracy. In this approach the kernel is not expanded on a set of functions derived from the LL eigenfunctions, and there are no instabilities in energy associated with a choice of functions breaking the $\gamma\leftrightarrow 1-\gamma$ symmetry, with γ being the variable Mellin–conjugate of the transverse momenta. This is explicitly shown at the left hand side of Fig. 13 where the coloured bands correspond to uncertainties from the choice of renormalisation scale. Since the exponential growth at NLL is slower than at LL, there is little overlap between the two predictions, and furthermore these move apart for increasing rapidities. The NLL corrections to the intercept amount to roughly 50% and are stable with increasing rapidities.

In transverse momentum space the NLL corrections are stable when the two transverse scales entering the forward gluon Green's function are of similar magnitude. However, when the ratio between these scales departs largely from unity, the perturbative convergence is poor, driving, as it is well–known, the gluon Green's function into an oscillatory behaviour with regions of negative values along the period of oscillation. This behaviour is demonstrated in the second plot of Fig 13.

The way the perturbative expansion of the BFKL kernel is improved by simultaneous resummation of energy and collinear logs has been discussed in sections 3.1,3.2. In particular, the original approach based on the introduction in the NLL BFKL kernel of an all order resummation of terms compatible with renormalisation group evolution described in ref. [60] (and incorporated in the CCSS approach of section 3.1) can be implemented in the iterative method here explained [69] (the method of ref. [60] was combined with the imposition of a veto in rapidities in refs. [70–72]). The main idea is that the solution to the ω–shift proposed in ref. [60]

$$
\omega = \bar{\alpha}_s\left(1+\left(\mathrm{a}+\frac{\pi^2}{6}\right)\bar{\alpha}_s\right)\left(2\psi(1)-\psi\left(\gamma+\frac{\omega}{2}-\mathrm{b}\,\bar{\alpha}_s\right)-\psi\left(1-\gamma+\frac{\omega}{2}-\mathrm{b}\,\bar{\alpha}_s\right)\right)
$$

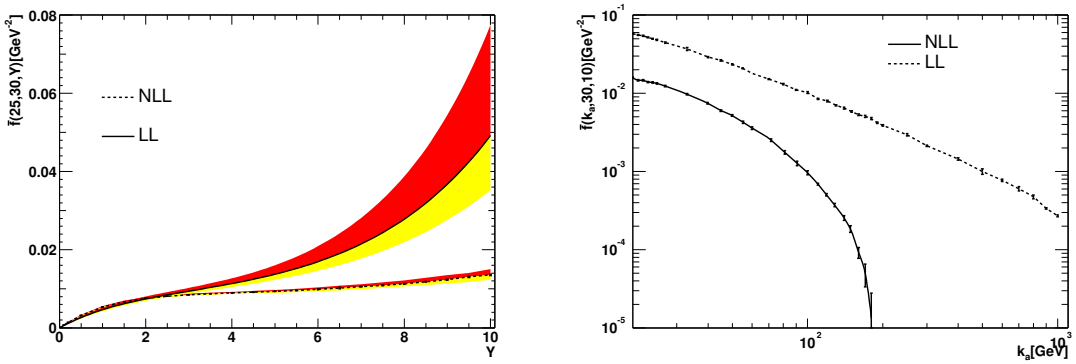

Fig. 13: Analysis of the gluon Green's function as obtained from the NLL BFKL equation. The plot to the left shows the evolution in rapidity of the gluon Green's function at LL and NLL for fixed $k_a = 25$ GeV and $k_b = 30$ GeV. The plot on the right hand side shows the dependence on k_a for fixed $k_b = 30$ GeV and $Y = 10$.

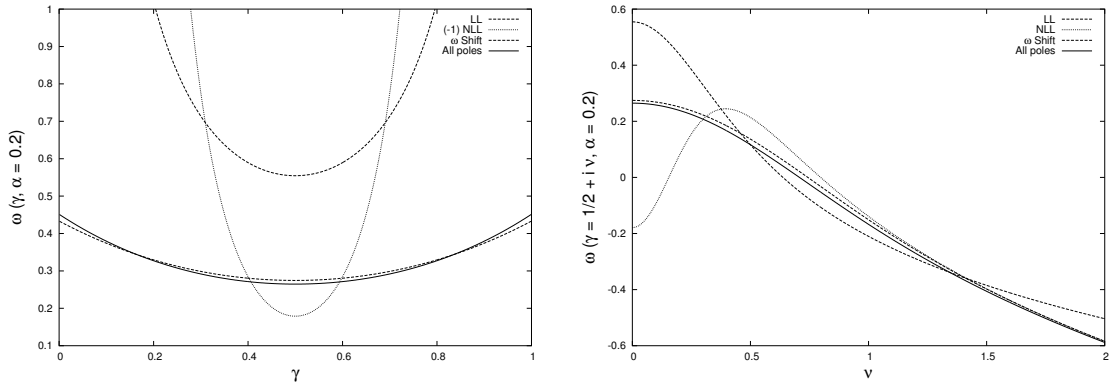

Fig. 14: The γ–representation of the LL and NLL scale invariant kernels together with the collinearly–improved kernel by an ω–shift and the "all–poles" resummation.

$$+ \quad \bar{\alpha}_s^2 \left(\chi_1(\gamma) + \left(\frac{1}{2}\chi_0(\gamma) - \mathrm{b} \right) \left(\psi'(\gamma) + \psi'(1-\gamma) \right) - \left(\mathrm{a} + \frac{\pi^2}{6} \right) \chi_0(\gamma) \right), \tag{29}$$

can be very accurately approximated by the sum of the approximated solutions to the shift at each of the poles in γ of the LL eigenvalue of the BFKL kernel. This provides an effective "solution" of Eq. (29) of the form [69]

$$\begin{aligned} \omega \;&=\; \bar{\alpha}_s\chi_0(\gamma) + \bar{\alpha}_s^2\chi_1(\gamma) + \left\{ \sum_{m=0}^{\infty} \left[\left(\sum_{n=0}^{\infty} \frac{(-1)^n (2n)!}{2^n n!(n+1)!} \frac{\left(\bar{\alpha}_s + \mathrm{a}\,\bar{\alpha}_s^2\right)^{n+1}}{\left(\gamma + m - \mathrm{b}\,\bar{\alpha}_s\right)^{2n+1}} \right) \right.\right. \\ &- \left.\left. \frac{\bar{\alpha}_s}{\gamma+m} - \bar{\alpha}_s^2 \left(\frac{\mathrm{a}}{\gamma+m} + \frac{\mathrm{b}}{(\gamma+m)^2} - \frac{1}{2(\gamma+m)^3} \right) \right] + \{\gamma \to 1-\gamma\} \right\}, \end{aligned} \tag{30}$$

where χ_0 and χ_1 are, respectively, the LL and NLL scale invariant components of the kernel in γ representation with the collinear limit

$$\chi_1(\gamma) \simeq \frac{\mathrm{a}}{\gamma} + \frac{\mathrm{b}}{\gamma^2} - \frac{1}{2\gamma^3}, \;\; \mathrm{a} = \frac{5}{12}\frac{\beta_0}{N_c} - \frac{13}{36}\frac{n_f}{N_c^3} - \frac{55}{36}, \;\; \mathrm{b} = -\frac{1}{8}\frac{\beta_0}{N_c} - \frac{n_f}{6N_c^3} - \frac{11}{12}. \tag{31}$$

The numerical solution to Eq. (29) and the value of expression (30) are compared in Fig. 14. The stability of the perturbative expansion is recovered in all regions of transverse momenta with a prediction for the intercept of 0.3 at NLL for $\bar{\alpha}_s = 0.2$, a result valid up to the introduction of scale invariance breaking

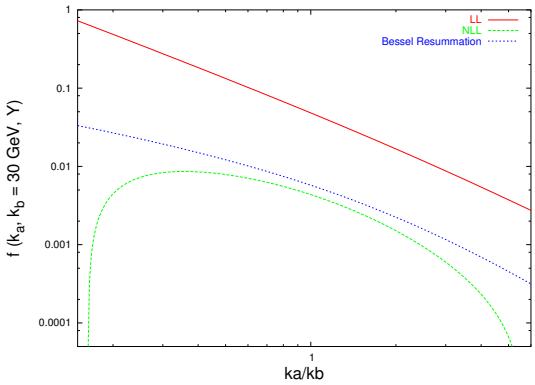

Fig. 15: The behaviour of the NLL gluon Green's function using the Bessel resummation.

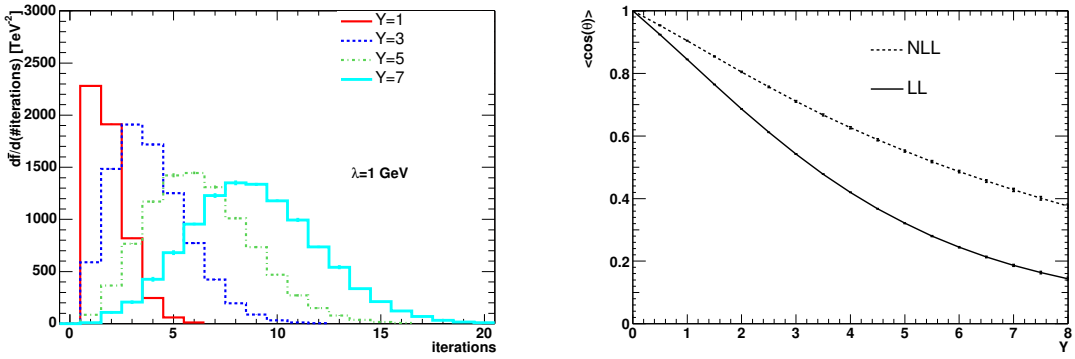

Fig. 16: Distribution in the number of iterations and angular dependence of the NLL gluon Green's function.

terms. The implementation of expression (30) in transverse momentum space is simple given that the transverse components decouple from the longitudinal in this form of the collinear resummation [69]. The prescription is to remove the term $-\frac{\bar{\alpha}_s^2}{4}\ln^2\frac{q^2}{k^2}$ from the real emission kernel, $\mathcal{K}_r\left(\vec{q},\vec{k}\right)$, and replace it with

$$\left(\frac{q^2}{k^2}\right)^{-\mathrm{b}\bar{\alpha}_s\frac{|k-q|}{k-q}}\sqrt{\frac{2\left(\bar{\alpha}_s+\mathrm{a}\,\bar{\alpha}_s^2\right)}{\ln^2\frac{q^2}{k^2}}}J_1\left(\sqrt{2\left(\bar{\alpha}_s+\mathrm{a}\,\bar{\alpha}_s^2\right)\ln^2\frac{q^2}{k^2}}\right)-\bar{\alpha}_s-\mathrm{a}\,\bar{\alpha}_s^2+\mathrm{b}\,\bar{\alpha}_s^2\frac{|k-q|}{k-q}\ln\frac{q^2}{k^2}, \quad (32)$$

with J_1 the Bessel function of the first kind. This prescription does not affect angular dependences and generates a well–behaved gluon Green's function as can be seen in Fig. 15 where the oscillations in the collinear and anticollinear regions of phase space are consistently removed. At present, work is in progress to study the effect of the running of the coupling in this analysis when the Bessel resummation is introduced in the iterative procedure of Ref. [67].

A great advantage of the iterative method here described is that the solution to the NLL BFKL equation is generated integrating the phase space using a Monte Carlo sampling of the different parton configurations. This allows for an investigation of the diffusion properties of the BFKL kernel as shown in ref. [73], and provides a good handle on the average multiplicities and angular dependences of the evolution. Multiplicities can be extracted from the Poisson–like distribution in the number of iterations of the kernel needed to reach a convergent solution, which is obtained numerically at the left hand side of Fig. 16 for a fixed value of the λ parameter. On the right hand side of the figure a study of the azimuthal angular correlation of the gluon Green's function is presented at $Y = 5$. This decorrelation will directly impact the prediction for the azimuthal angular decorrelation of two jets with a large rapidity separation, in a fully inclusive jet sample (i.e. no rapidity gaps). The increase of the angular correlation when the NLL terms are included is a characteristic feature of these corrections. This study is possible using this

approach because the NLL kernel is treated in full, without angular averaging, so there is no need to use a Fourier expansion in angular variables.

References

[1] S. Moch et al., *Precision predictions for deep-inelastic scattering*. These proceedings.

[2] Sterman, G., Nucl. Phys. **B281**, 310 (1987).

[3] Catani, S. and Trentadue, L., Nucl. Phys. **B327**, 323 (1989).

[4] Forte, S. and Ridolfi, G., Nucl. Phys. **B650**, 229 (2003).

[5] Vogt, A., Phys. Lett. **B497**, 228 (2001).

[6] Moch, S. and Vermaseren, J. A. M. and Vogt, A., Nucl. Phys. **B688**, 101 (2004).

[7] Moch, S. and Vermaseren, J. A. M. and Vogt, A., Nucl. Phys. **B726**, 317 (2005).

[8] Moch, S. and Vogt, A., *Higher-order soft corrections to lepton pair and higgs boson production*. Preprint hep-ph/0508265, 2005.

[9] Laenen, E. and Magnea, L., *Threshold resummation for electroweak annihilation from dis data*. Preprint hep-ph/0508284, 2005.

[10] Eynck, T. O. and Laenen, E. and Magnea, L., JHEP **06**, 057 (2003).

[11] Gribov, V.N. and Lipatov, L.N., Sov.J.Nucl.Phys **15**, 438 (1972).

[12] Altarelli, G. and Parisi, G., Nucl.Phys. **B126**, 298 (1977).

[13] Dokshitzer, Yu. L., JETP **46**, 641 (1977).

[14] Lipatov, L. N., Sov. J. Nucl. Phys. **23**, 338 (1976).

[15] Kuraev, E. A. and Lipatov, L. N. and Fadin, Victor S., Sov. Phys. JETP **45**, 199 (1977).

[16] Balitsky, I. I. and Lipatov, L. N., Sov. J. Nucl. Phys. **28**, 822 (1978).

[17] Lipatov, L. N., Sov. Phys. JETP **63**, 904 (1986).

[18] Vogt, A. and Moch, S. and Vermaseren, J. A. M., Nucl. Phys. **B691**, 129 (2004).

[19] Camici, G. and Ciafaloni, M., Phys. Lett. **B412**, 396 (1997).

[20] Ciafaloni, M. and Camici, G., Phys. Lett. **B430**, 349 (1998).

[21] Ciafaloni, M. and Colferai, D. and Salam, G. P., Phys. Rev. **D60**, 114036 (1999).

[22] Ciafaloni, M. and Colferai, D. and Colferai, D. and Salam, G. P. and Stasto, A. M., Phys. Lett. **B576**, 143 (2003).

[23] Ciafaloni, M. and Colferai, D. and Salam, G. P. and Stasto, A. M., Phys. Rev. **D68**, 114003 (2003).

[24] Altarelli, G. and Ball, R. D. and Forte, S., Nucl. Phys. **B575**, 313 (2000).

[25] Altarelli, G. and Ball, R. D. and Forte, S., Nucl. Phys. **B599**, 383 (2001).

[26] Altarelli, G. and Ball, R. D. and Forte, S., Nucl. Phys. **B621**, 359 (2002).

[27] Altarelli, G. and Ball, R. D. and Forte, S., Nucl. Phys. **B674**, 459 (2003).

[28] Altarelli, G. and Ball, R. D. and Forte, S., *An improved splitting function for small x evolution*. Preprint hep-ph/0310016, 2003.

[29] Altarelli, G. and Ball, R. D. and Forte, S., Nucl. Phys. Proc. Suppl. **135**, 163 (2004).

[30] Altarelli, G. and Ball, R. D. and Forte, S., *Perturbatively stable resummed small x kernels*. Preprint CERN-PH-TH/2005-174, 2005.

[31] Catani, S. and Mangano, Michelangelo L. and Nason, Paolo and Oleari, Carlo and Vogelsang, Werner, JHEP **03**, 025 (1999).

[32] Laenen, E. and Sterman, G. and Vogelsang, W., Phys. Rev. Lett. **84**, 4296 (2000).

[33] Kidonakis, N. and Sterman, G., Nucl. Phys. **B505**, 321 (1997).

[34] Kidonakis, N. and Owens, J. F., Phys. Rev. **D63**, 054019 (2001).

[35] Laenen, E. and Moch, S., Phys. Rev. **D59**, 034027 (1999).
[36] Corcella, G. and Mitov, A. D., Nucl. Phys. **B676**, 346 (2004).
[37] A. Cooper-Sarkar, C. Gwenlan, *Comparison and combination of zeus and h1 pdf analyses*. These proceedings.
[38] S. I. Alekhin, *Towards precise determination of the nucleon pdfs*. These proceedings.
[39] Alekhin, S., *Parton distribution functions from the precise nnlo qcd fit*. Preprint hep-ph/0508248, 2005.
[40] Tzanov, M. et al., *New qcd results from nutev*. Preprint hep-ex/0306035, 2003.
[41] Naples, D. et al., *Nutev cross section and structure function measurements*. Preprint hep-ex/0307005, 2003.
[42] Arneodo, M. et al., Nucl. Phys. **B483**, 3 (1997).
[43] Benvenuti, A. C. et al., Phys. Lett. **B223**, 485 (1989).
[44] Benvenuti, A. C. et al., Phys. Lett. **B237**, 592 (1990).
[45] Forte, S. and Garrido, L. and Latorre, J. I. and Piccione, A., JHEP **05**, 062 (2002).
[46] Del Debbio, L. and Forte, S. and Latorre, J. I. and Piccione, A. and Rojo, J., JHEP **03**, 080 (2005).
[47] Corcella, G. and Magnea, L., *Soft-gluon resummation effects on parton distributions*. Preprint hep-ph/0506278, 2005.
[48] Pumplin, J. et al., JHEP **07**, 012 (2002).
[49] Fadin, V. S. and Lipatov, L. N., Phys. Lett. **B429**, 127 (1998).
[50] Ciafaloni, M. and Colferai, D., *Dimensional regularisation and factorisation schemes in the bfkl equation at subleading level*. Preprint hep-ph/0507106, 2005.
[51] Ball, R. D. and Forte, S., Phys. Lett. **B465**, 271 (1999).
[52] Catani, S. and Ciafaloni, M. and Hautmann, F., Phys. Lett. **B242**, 97 (1990).
[53] Catani, S. and Ciafaloni, M. and Hautmann, F., Nucl. Phys. **B366**, 135 (1991).
[54] Collins, J. C. and Ellis, R. K., Nucl. Phys. **B360**, 3 (1991).
[55] Bartels, J. and Gieseke, S. and Qiao, C. F., Phys. Rev. **D63**, 056014 (2001).
[56] Bartels, J. and Gieseke, S. and Kyrieleis, A., Phys. Rev. **D65**, 014006 (2002).
[57] Bartels, J. and Colferai, D. and Gieseke, S. and Kyrieleis, A., Phys. Rev. **D66**, 094017 (2002).
[58] Bartels, J. and Colferai, D. and Vacca, G. P., Eur. Phys. J. **C24**, 83 (2002).
[59] Bartels, J. and Colferai, D. and Vacca, G. P., Eur. Phys. J. **C29**, 235 (2003).
[60] Salam, G. P., JHEP **07**, 019 (1998).
[61] Ciafaloni, M. and Colferai, D., Phys. Lett. **B452**, 372 (1999).
[62] Ciafaloni, M. and Colferai, D. and Salam, G. P., JHEP **07**, 054 (2000).
[63] Ball, R. D. and Forte, S., Phys. Lett. **B405**, 317 (1997).
[64] Catani, S. and Hautmann, F., Nucl. Phys. **B427**, 475 (1994).
[65] Ball, R. D. and Forte, S., Phys. Lett. **B359**, 362 (1995).
[66] Ciafaloni, M. and Colferai, D. and Salam, G. P. and Stasto, A. M., Phys. Lett. **B587**, 87 (2004).
[67] Andersen, J. R. and Sabio Vera, A., Phys. Lett. **B567**, 116 (2003).
[68] Andersen, J. R. and Sabio Vera, A., Nucl. Phys. **B679**, 345 (2004).
[69] Sabio Vera, A., Nucl. Phys. **B722**, 65 (2005).
[70] Schmidt, C. R., Phys. Rev. **D60**, 074003 (1999).
[71] Forshaw, J. R. and Ross, D. A. and Sabio Vera, A., Phys. Lett. **B455**, 273 (1999).
[72] Chachamis, G. and Lublinsky, M. and Sabio Vera, A., Nucl. Phys. **A748**, 649 (2005).
[73] Andersen, J. R. and Sabio Vera, A., JHEP **01**, 045 (2005).